*Published online 15 July 2013* *Nucleic Acids Research, 2013, Vol. 41, No. 17* ***8135–8143***
*doi:10.1093/nar/gkt611*

# Global 'bootprinting' reveals the elastic architecture of the yeast TFIIIB–TFIIIC transcription complex *in vivo*

**V. Nagarajavel, James R. Iben, Bruce H. Howard, Richard J. Maraia* and David J. Clark***

Program in Genomics of Differentiation, Eunice Kennedy Shriver National Institute for Child Health and Human Development, National Institutes of Health, Bethesda, MD, USA

Received May 9, 2013; Revised June 14, 2013; Accepted June 20, 2013

## ABSTRACT

**TFIIIB and TFIIIC are multi-subunit factors required for transcription by RNA polymerase III. We present a genome-wide high-resolution footprint map of TFIIIB–TFIIIC complexes in *Saccharomyces cerevisiae*, obtained by paired-end sequencing of micrococcal nuclease-resistant DNA. On tRNA genes, TFIIIB and TFIIIC form stable complexes with the same distinctive occupancy pattern but in mirror image, termed 'bootprints'. Global analysis reveals that the TFIIIB–TFIIIC transcription complex exhibits remarkable structural elasticity: tRNA genes vary significantly in length but remain protected by TFIIIC. Introns, when present, are markedly less protected. The RNA polymerase III transcription terminator is flexibly accommodated within the transcription complex and, unexpectedly, plays a major structural role by delimiting its 3′-boundary. The *ETC* sites, where TFIIIC binds without TFIIIB, exhibit different bootprints, suggesting that TFIIIC forms complexes involving other factors. We confirm six *ETC* sites and report a new site (*ETC10*). Surprisingly, TFIIIC, but not TFIIIB, interacts with some centromeric nucleosomes, suggesting that interactions between TFIIIC and the centromere may be important in the 3D organization of the nucleus.**

## INTRODUCTION

Massively parallel sequencing has been used to sequence nucleosomes genome-wide in various organisms. The budding yeast, *Saccharomyces cerevisiae*, is particularly amenable to such analysis because its relatively small genome can be sequenced in great depth, revealing crucial details. The basic experiment is to digest chromatin extensively with micrococcal nuclease (MNase) to obtain nucleosome core particles, which contain ~147 bp of DNA wrapped around a central octamer of core histones (two each of H2A, H2B, H3 and H4) (1) and then sequence the purified DNA. Thus, a nucleosome is operationally defined by the protection of ~147 bp of DNA from MNase. This definition is entirely adequate in the study of *in vitro* nucleosome reconstitution systems using purified components. However, *in vivo* there may be other protein–DNA complexes that protect ~150 bp of DNA from MNase digestion, which might therefore masquerade as nucleosomes. We show here that this is the case for transcription factor complexes formed on tRNA genes.

tRNA genes are transcribed by RNA polymerase III (Pol III) with the aid of two multi-subunit transcription factors, TFIIIC and TFIIIB (2). Budding yeast TFIIIC has six subunits (Tfc1, 3, 4, 6, 7 and 8), whereas TFIIIB has three subunits (Brf1, Bdp1 and the TATA binding protein). TFIIIC binds specifically to two internal promoter elements: the A and B boxes. TFIIIC recruits TFIIIB, which binds upstream of the tRNA gene, forming a stable pre-initiation complex that is recognized by Pol III. Pol III also transcribes a few other non-coding RNA genes, for which TFIIIB and TFIIIC are required.

tRNA genes and TFIIIC also have unexpected roles in chromatin structure, including barrier and insulator functions (3,4), the silencing of neighboring Pol II genes (5–7) and in fission yeast, TFIIIC sites prevent the spread of heterochromatin and also mediate the tethering of chromosomes to the nuclear periphery (8).

Previously, we described genome-wide nucleosome maps for budding yeast obtained using paired-end sequencing (9–11), which provides short reads from both

*To whom correspondence should be addressed. Tel: +1 301 496 6966; Fax: +1 301 480 1907; Email: clarkda@mail.nih.gov
Correspondence may also be addressed to Richard J. Maraia. Tel: +1 301 402 3567; Fax: +1 301 480 9354; Email: maraiar@mail.nih.gov
Present address:
V. Nagarajavel, Genomic Medicine Institute, Lerner Research Institute NE50, 9500 Euclid Ave, Cleveland, OH 44195, USA.

Published by Oxford University Press 2013. This work is written by US Government employees and is in the public domain in the US.

ends of each DNA molecule, allowing the length of the DNA fragment to be deduced after alignment to the genome sequence. We found that, in general, canonical nucleosomes are not precisely positioned with respect to the DNA sequence. Instead, there is significant heterogeneity in positioning within a population of haploid yeast cells. This 'fuzzy' positioning is indicated by the generally rounded peaks observed in nucleosome occupancy maps. However, a notable exception is the single centromeric nucleosome on each chromosome, which is positioned identically in all cells, as revealed by a single squared-off peak over the centromere in the nucleosome occupancy map (10,12). Centromeric nucleosomes certainly differ from canonical nucleosomes in that they contain CenH3 in place of H3, but their precise composition is controversial (13).

Here, we describe similar square peaks at tRNA genes. We show that they correspond to stable TFIIIB–TFIIIC complexes, which protect ~150 bp of DNA from MNase. We have mapped all stable TFIIIC- and TFIIIB-containing complexes in the yeast genome with high precision, deriving information similar to that obtained by classical footprinting. Notably, these 'bootprints' indicate that the Pol III transcription terminator plays a major role in the structure by determining the 3′-boundary. The Pol III transcription complex has a remarkably elastic structure that allows it to accommodate tRNA genes that differ in length owing to variable distances between the A and B boxes and between the B-box and the transcription terminator. Surprisingly, TFIIIC also interacts with some centromeric nucleosomes, suggesting a physical link between TFIIIC and the centromere.

## MATERIALS AND METHODS

### Nucleosome maps

JRY4013 (W303 ***MATα*** *can1-100 his3-11,15 leu2-3,112 lys2Δ trp1-1 ura3-1)* (14) was provided by Rohinton Kamakaka. Cells were grown to an $OD_{600}$ of ~0.5 in synthetic complete medium. Core particle DNA was prepared from nuclei digested with MNase as described (9).

### Immuno-purification of TFIIIB and TFIIIC complexes from MNase-digested nuclei

Three W303 yeast strains were provided by David Donze: DDY4 (no-tag control), DDY1389 (Flag-tagged Tfc1) and DDY4381 (Flag-tagged Brf1) (15). Nuclei were digested to mono-nucleosomes with MNase as above, except that digestion was stopped by adding Na-EDTA, pH 7.5, to 5 mM, Na-EGTA to 5 mM and Triton X100 to 0.05%, to preserve the chromatin. The extent of digestion was verified by analysis of the DNA in an agarose gel. Nuclear debris was removed by centrifugation (1 min at 12 000*g*). The supernatant was filtered using a centrifugal filter (Millipore Ultrafree-MC, 0.45 μm; UFC30HV25) and incubated with anti-Flag antibody attached to Sepharose beads (Sigma A2220) for 30 min at 4°C with rotation. The resin was collected by a brief spin; unbound chromatin was removed. The beads were washed thrice with 0.15 M NaCl, 10 mM Tris–HCl, pH 8.0, 0.05% NP40, 1 mM Na-EGTA containing protease inhibitors (Roche 11873580001). Bound chromatin was eluted with 0.8 mg/ml 3-Flag peptide (Sigma F4799) in wash buffer. DNA was extracted from the input and the eluted chromatin immunoprecipitate (IP) and ligated to Illumina paired-end adaptors (9). Ligated adaptor dimers were removed by gel-purification of all larger ligation products. Input DNA was amplified using 14 PCR cycles. IP-DNA was amplified using 24–28 cycles, gel-purified and re-amplified using 14 cycles (re-amplification was necessary because of contaminating adaptor dimer).

### Paired-end sequencing

Sequencing was performed by the NHLBI DNA Sequencing Core Facility. Paired reads were aligned to the SacCer2 version of the *S. cerevisiae* genome using either BWA (16) or Bowtie2 (17). Numbers of aligned paired reads for biological replicate experiments were as follows: nucleosomes (9.4 and 9.2 million), Tfc1-Input (51.4 and 4.0 million), Tfc1-IP (3.5 and 82.8 million), Brf1-Input (20.8 and 53.5 million), Brf1-IP (13.0 and 16.4 million), Control-Input (25.0 million) and Control-IP (9.3 million). Occupancy maps were constructed as described (10,12). The data have been deposited at the GEO database (GSE44586). tRNA genes were identified using tRNAscan-SE (18). A custom Perl program was used to predict terminators in downstream sequences based on the occurrence of four or more consecutive T residues. Sequence logos were generated using WebLOGO (19).

## RESULTS

### Chromatin structure of the tRNA genes

Yeast nuclei were digested to nucleosome core particles with MNase, and gel-purified DNA of ~150 bp was subjected to paired-end sequencing. We searched the resulting nucleosome occupancy map for square peaks, which may indicate the presence of unusual chromatin structures. We found square peaks at half of the 275 tRNA genes: two examples are shown: *EMT5* and *tT(UGU)G2* (Figure 1A). Most of the tRNA genes lacking square peaks exhibited little or no signal and therefore had been fully digested by MNase, or showed irregular peaks.

The square peak at each tRNA gene could represent either an unusually well-positioned nucleosome (like the *CEN* nucleosome), or a protein–DNA complex that protects a length of DNA similar to that of the nucleosome. Two lines of evidence suggested the latter interpretation: (i) Previous studies using histone ChIP-chip (20) or nucleosome ChIP-seq after IP with anti-histone antibodies (21,22) indicate that tRNA genes are heavily depleted of histones; (ii) tRNA genes form stable TFIIIB–TFIIIC transcription complexes *in vitro* (23,24); TFIIIC binds tightly and specifically to the internal A- and B-box promoter elements within each tRNA gene. Specific binding can account for the square peak because all complexes would be positioned similarly with respect to the DNA sequence. Therefore, we asked whether the

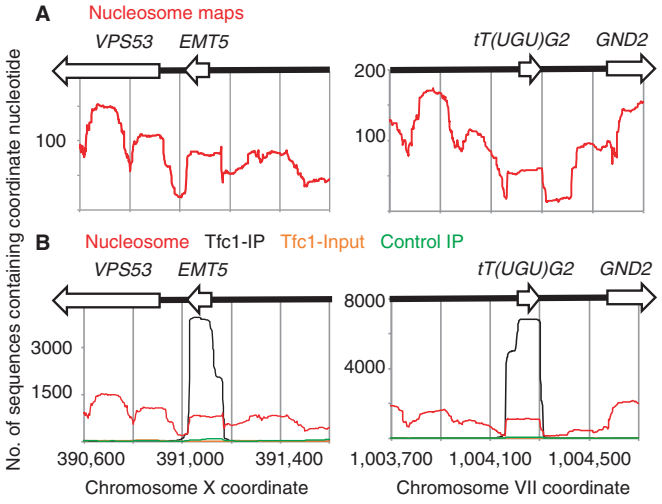


**Figure 1.** Nucleosome-like complexes on yeast tRNA genes contain Tfc1. (**A**) Nucleosome occupancy maps for two typical short tRNA genes, *EMT5* and *tT(UGU)G2*, showing the distinctive square peak over the tRNA gene. (**B**) Tfc1 bootprints on the same tRNA genes. Tfc1-Flag IP (black line); Tfc1-input (orange line); control IP (green line). Nucleosome maps in *A* and *B* are superimposed after multiplying the actual number of sequences by 10 (red line) to highlight the correspondence between the square peaks in the nucleosome map and the Tfc1 occupancy peaks.

nucleosome-like structures on the tRNA genes contain TFIIIC.

To address this question, we used a yeast strain carrying Flag-tagged Tfc1, a TFIIIC subunit. Nuclei from Tfc1-Flag and control (no tag) cells were digested to mono-nucleosomes with MNase, the reaction was stopped with EGTA and Tfc1-Flag complexes were immuno-purified using anti-Flag antibody. Bound complexes were eluted with Flag peptide and the purified DNA was subjected to paired-end sequencing. Input DNA samples were also sequenced. The sequences obtained were used to create a Tfc1 occupancy plot.

If the nucleosome-like structures over the tRNA genes include TFIIIC complexes, we would expect to observe square peaks over the tRNA genes in the Tfc1-IP. This was the case: there was a strong enrichment of Tfc1 over *EMT5* and *tT(UGU)G2* (Figure 1B). In fact, the signal over the tRNA gene was ~5000 sequences, whereas the background was ~20. The almost vertical boundaries of the complex coincided closely with those of the square peaks observed in the nucleosome map (Figure 1). The fact that the entire tRNA gene was protected suggests that intact TFIIIC was immuno-purified, not just Tfc1, consistent with the stability of the TFIIIC complex in the absence of DNA (25).

The shape of the protected region in the occupancy plot was distinctive, resembling a boot (Figure 1B). Because the information it represents is similar to that obtained from a classical footprinting experiment, we named this feature a 'bootprint'. The Tfc1 bootprint comprised two populations of DNA fragments, which differ in length. The long and short fragments share similar 3′-ends with respect to the tRNA gene, but they give two distinct well-defined boundaries at the 5′-end of the tRNA gene (Figure 1B). The short fragments correspond to the entire tRNA gene; previous work *in vitro* suggests that these fragments represent protection due to TFIIIC (26). The longer fragments correspond to the entire tRNA gene plus the upstream region. Because TFIIIB is recruited to the upstream region of tRNA genes (26), the longer fragments most likely represent protection due to the TFIIIB–TFIIIC complex. The inference is that MNase might occasionally cleave between TFIIIC and TFIIIB, resulting in the shorter DNA fragments.

We note that the bootprint is not the same shape as the square peak in the nucleosome map, even though the outer boundaries coincide almost exactly. This is because DNA of mono-nucleosomal size was gel-purified for the nucleosome map, resulting in exclusion of shorter DNA fragments, whereas a wider range of DNA fragments was purified from the gel for the Tfc1-IP (Supplementary Figure S1).

## Global analysis of TFIIIC bootprints

We undertook a global analysis of all tRNA genes to determine the general features of TFIIIC bootprints. Yeast tRNA genes have the same basic organization but vary in length (Figure 2A). The first nucleotide in the mature tRNA was designated as +1 because the transcription start site has not been mapped for most tRNA genes. The locations of the A and B boxes are fixed with respect to +1 and the 3′-end of the mature tRNA, respectively. Thus, the variability in tRNA gene length derives from insertions between the A and B boxes, in the variable arm of the tRNA and/or as an intron, and also in a second region, between the B-box and the transcription terminator (3′-trailer).

Inspection of individual tRNA genes suggested that the length of the bootprint depended on the length of the gene. Consequently, the 275 tRNA genes were divided into three groups: (i) intron-less tRNA genes of 71–74 bp (192 genes); (ii) intron-less tRNA genes of 82–84 bp (22 genes); (iii) intron-containing tRNA genes of 89–133 bp (61 genes). The terminal nucleotides of each sequenced DNA fragment represent the MNase cut sites. The number of DNA fragments terminating at a given nucleotide from −200 to +200 was summed and expressed as a fraction of the total number of Tfc1-IP fragments for each gene. The data for all genes in each size-class were summed and divided by the number of genes in the size-class. The result is a map of the average locations of the major MNase cut sites for each class of tRNA gene.

An example of the first class of tRNA gene is *tG(GCC)G1*, a 71-bp glycyl-tRNA (Figure 2B). The global map indicated major cut sites at −56, −13, −2 and +85 (Figure 2E). The cuts at −56 and +85 correspond to the outer boundaries of the complex and protected DNA fragments of ~142 bp (similar in size to the nucleosome). The major internal cut sites were at −13 and −2. The tRNA transcription unit was completely protected from digestion.

An example of the second class of tRNA gene is *SUP16*, an 82-bp seryl-tRNA (Figure 2C). Major cut sites were

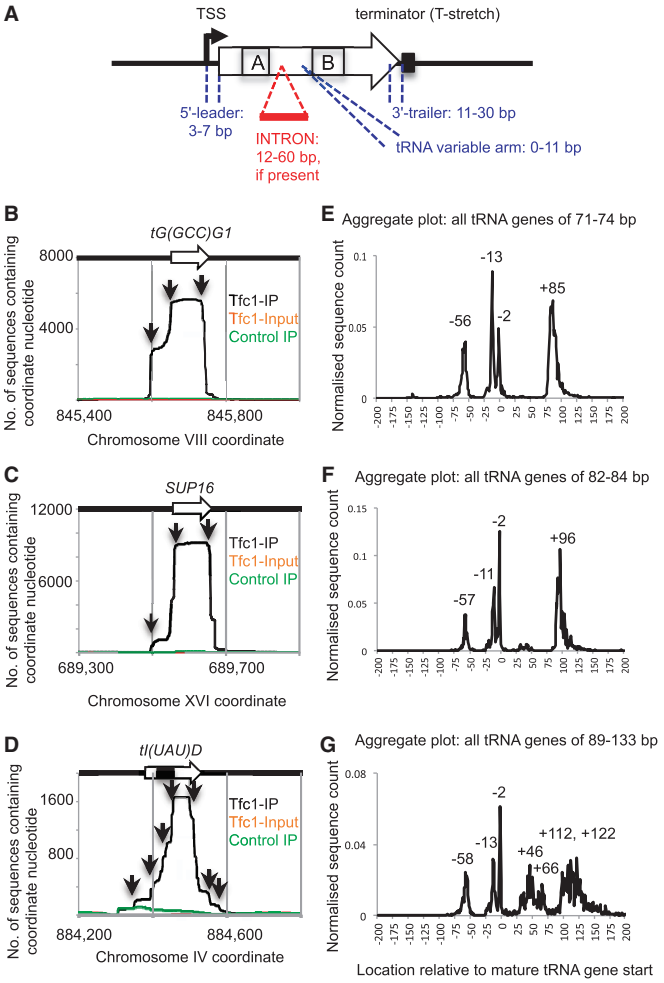


**Figure 2.** Global analysis of Tfc1 bootprints on tRNA genes. (**A**) Anatomy of a yeast tRNA gene. The 275 tRNA genes were divided into three classes, depending on their lengths. Representative examples of Tfc1 bootprints (black line) are shown for each class: (**B**) *tG(GCC)G1* for the 71–74 bp class (192 genes); (**C**) *SUP16* for the 82–84 bp class (22 genes); (**D**) *tI(UAU)D* for the 89–133 bp class (61 genes with introns). The Tfc1-input (orange) and control IP (green) were normalized to the total number of aligned sequences obtained for the Tfc1-IP. Major MNase cut sites are indicated by arrows. (**E–G**) Global maps of the major MNase cut sites defining the Tfc1 bootprints for all genes in the three tRNA gene length classes. The most prominent peaks are marked relative to the first nucleotide of the mature tRNA at +1.

observed at −56, −11, −2 and +96 (Figure 2F). The cuts at −56 and +96 correspond to the outer boundaries of the complex and protected DNA fragments of ∼153 bp. Therefore, the protected region is ∼11 bp longer than that observed for the short tRNA genes. Because the upstream boundary was the same in both cases (−56) and so were the internal cut sites, whereas the downstream boundary shifted downstream by ∼11 bp, the expanded protection corresponds to the increased length of the tRNA gene (10–13 bp).

The longest tRNA gene is *tI(UAU)D*, a 133-bp isoleucyl-tRNA, which includes a 60-bp intron (Figure 2D). Global analysis of intron-containing tRNA genes revealed major cut sites at −56, −13, −2 and at a series of locations from +30 to +66 and from +100 to +122 (Figure 2G). Thus, the upstream boundary at −56 and the major internal cut sites at −13 and −2 were the same as for the other tRNA genes, but the downstream boundary was diffuse, reflecting the wide range in gene length (89–133 bp). Most striking was the appearance of internal cut sites within the tRNA gene. These occurred within introns and imply that the protection of intronic DNA afforded by TFIIIC is significantly weaker than that of the rest of the gene.

## Global analysis of TFIIIB bootprints

TFIIIB is recruited by TFIIIC to the upstream region of tRNA genes (26). Given that the Tfc1 bootprint includes the upstream region, it appears that TFIIIC and TFIIIB form a stable complex on tRNA genes *in vivo*. To confirm that the upstream portion of the Tfc1 bootprint corresponds to protection by TFIIIB, we repeated the immunopurification using a strain with Flag-tagged Brf1 (a TFIIIB subunit).

The Brf1 bootprint was similar in shape to that of Tfc1, except that it was almost its mirror-image, with the shorter and longer DNA fragments having the same 5′-end but different 3′-ends with respect to the tRNA (Figure 3A–C). This observation can be explained if the internal MNase cut sites are located between TFIIIB and TFIIIC, such that the IP for Tfc1 pulled down the 3′-fragment, whereas the IP for Brf1 pulled down the 5′-fragment. This effect was more obvious with the longer tRNA genes: a gap appeared between the Brf1 and Tfc1 peaks at *tI(UAU)D*, corresponding to the intron (Figure 3C). The boundaries of the Brf1 bootprint were almost coincident with those of the Tfc1 bootprint, though not so sharply defined, probably because the Brf1-IP sample was less digested than the Tfc1-IP (Supplementary Figure S1).

Global analysis of the bootprints for the three different size-classes of tRNA gene showed that the upstream boundary of the TFIIIB-containing complex was located at −60, irrespective of gene length, and correlated well with that of the Tfc1 bootprint (Figure 3D–F). The downstream boundary of the Brf1 bootprint also coincided with that of Tfc1, indicating that TFIIIB and TFIIIC are bound together to form a stable complex. The internal cut sites for Brf1 were different from those observed for Tfc1: particularly at +13 and +21 in the shortest genes and at +21 and +43 in genes of intermediate length. All of these sites were observed for the longest genes, together with additional peaks within the intron, which did coincide with those observed for Tfc1 (Figure 3F). The apparent difference in internal MNase cut sites observed in the Brf1 and Tfc1 IPs might be due to differential loss of short DNA fragments during purification. If so, all of the observed cleavage sites indicate points of accessibility to MNase.

In conclusion, the Tfc1 and Brf1 bootprints are consistent with a stable TFIIIB–TFIIIC complex formed on all tRNA genes, with an upstream boundary close to −56 and a downstream boundary determined by the length of the tRNA gene. The data are consistent with classical studies

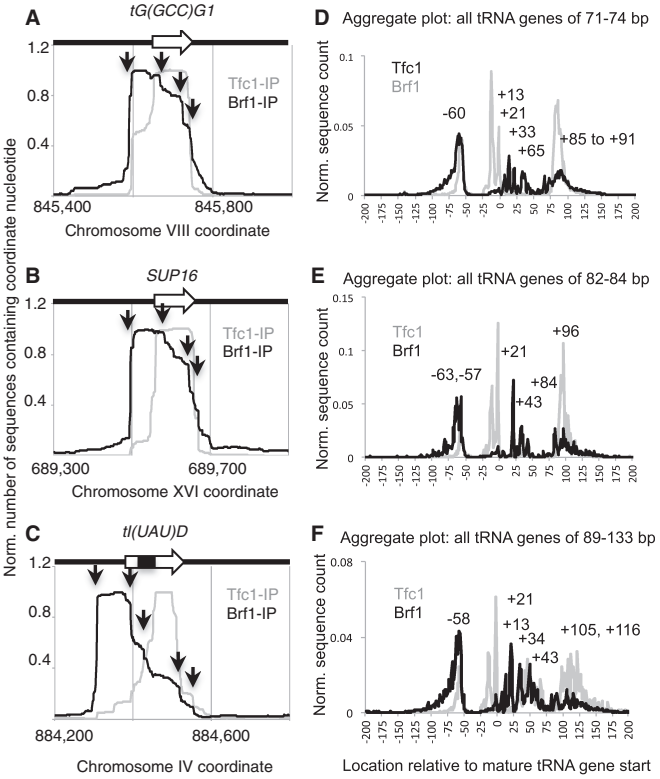


**Figure 3.** Global analysis of Brf1 bootprints on tRNA genes. Representative examples of Brf1-Flag (black line) and Tfc1-Flag bootprints (gray line) are shown for each tRNA size-class: (**A**) 71–74 bp; (**B**) 82–84 bp; (**C**) 89–133 bp. To compare the TFIIIB and TFIIIC bootprints, the highest signal for each complex was set at 1. Major MNase cut sites in the Brf1 IP are indicated by arrows. (**D–F**) Global maps of the major MNase cleavage sites defining the Tfc1 (gray) and Brf1 (black) bootprints for each tRNA gene length class. The most prominent peak positions in the Brf1 bootprint are marked relative to the first nucleotide of the mature tRNA at +1.

indicating that TFIIIB binds over the upstream region and TFIIIC binds over the gene itself.

### The transcription terminator delimits the 3′-boundary of the TFIIIC complex

What determines the downstream boundary of the TFIIIC complex? The most obvious possibility is that specific binding of the TFIIIC complex results in a boundary located at a fixed distance downstream of the B-box (Figure 2A). However, the distance from the B-box to the 3′-terminal nucleotide in the mature tRNA is invariant at 20 bp, which predicts that the boundary would also be invariant, but this is not the case (see below). An alternative candidate is the terminator. Efficient termination by Pol III is dependent on a stretch of T-residues variably located <20 bp from the 3′-end of the mature tRNA (27–29). Accordingly, we examined the relationship between the downstream boundary of the Tfc1 bootprint and the location of the T-stretch. Only tRNA genes with an uninterrupted downstream T-stretch of four or more residues were selected for analysis (81 genes). These genes were classified according to the distance between the 3′-end of the mature tRNA (which is fixed for all tRNA genes) and the 3′-end of the T-stretch, at single-nucleotide resolution (from 8 to 14 bp). The locations of the 3′-ends of the Tfc1-IP DNA fragments were mapped with respect to the 3′-end of the mature tRNA for each class of gene (Figure 4A). For example, for the 10 genes with a T-stretch ending 8 bp from the 3′-end of the mature tRNA, maximum cleavage by MNase occurred 11 bp from the 3′-end of the tRNA gene. The major MNase cut site shifted downstream as the T-stretch shifted downstream, such that the major cut was always 2 or 3 bp downstream of the 3′-end of the T-stretch and was therefore not set by the B box alone (Figure 4B). We conclude that the downstream boundary of the TFIIIC complex is fixed by the terminator. The T-stretch is located within the complex and is protected from digestion.

### TFIIIC bootprints at *ETC* sites and detection of a novel *ETC* site

TFIIIC has other roles, independent of transcription, involving binding at *ETC* sites ('extra TFIIIC sites'), identified by ChIP (30,31). *ETC* sites are bound by TFIIIC but not by TFIIIB or Pol III. We confirmed the presence of TFIIIC at six of the nine *ETC* sites reported in budding yeast. As expected, TFIIIB was not present at *ETC2*, *ETC6*, *ETC7* or *ETC8* (Figure 5A). A Brf1 signal was confirmed for TFIIIB at *ETC9* [a vestigial tRNA gene (32,33)] and at *ETC5* (32) (Supplementary Figure S2). In addition, we discovered a new *ETC* site, which we designated *ETC10* (Figure 5A); it contains a good predicted B-box (GCTCGAACA).

The Tfc1 signal at *ETC* sites was weak relative to tRNA genes, as shown by the ~10-fold lower number of sequences obtained. This might reflect weaker binding by TFIIIC because *ETC* sites have a B box but no A box (31). Weak binding and/or the fact that we did not cross-link with formaldehyde might explain why we did not detect Tfc1 at *ETC1*, *ETC3* or *ETC4*. It is unlikely that a sub-complex of TFIIIC is bound at these sites because various ChIP studies have together confirmed the presence of all six subunits of TFIIIC (30,31,34,35).

The Tfc1 bootprints at *ETC* sites were different from those observed at tRNA genes. The *ETC2*, *ETC6* and *ETC10* bootprints were fairly square and only 70–90 bp wide. These complexes might be TFIIIC bound by itself, but other factors may be present. The Tfc1 bootprints at *ETC7* and *ETC8* were different. The outer boundaries of *ETC8* indicated protection of ~230 bp, with stronger protection on one side, as shown by a tall narrow projection ~60 bp wide. The *ETC8* bootprint probably represents a complex of TFIIIC with an unknown factor.

### TFIIIC interacts with centromeric nucleosomes

Remarkably, a search for additional bootprints revealed the presence of centromeric (*CEN*) DNA in the Tfc1-IP (Figure 5B). Centromeric nucleosomes are readily identifiable by the square peak in the occupancy plot and by their fixed position with respect to *CEN* DNA (10,12). The boundaries of the Tfc1-complexes observed here coincided precisely with those of the *CEN* nucleosomes in the nucleosome map (Figure 5B) and with those reported

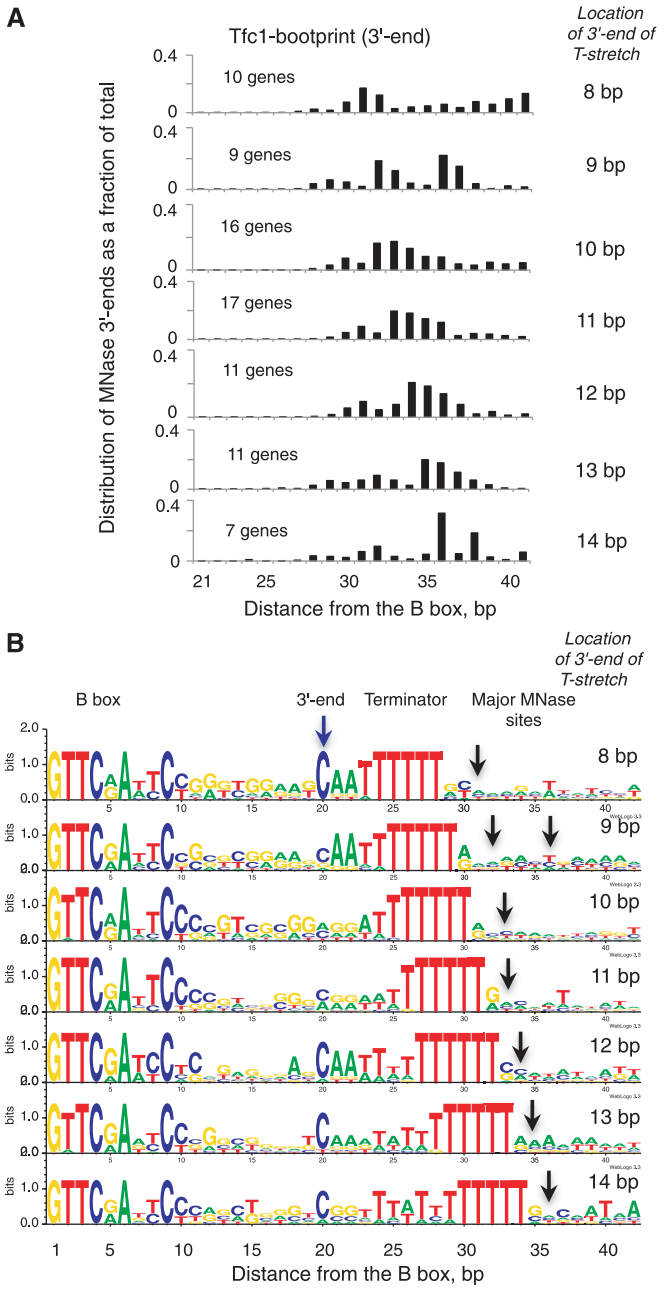


**Figure 4.** The 3′-boundary of the Tfc1 bootprint is located 2 or 3 bp downstream of the Pol III transcription terminator. tRNA genes with unambiguous terminators (T-stretches of at least four residues) were divided into classes according to the distance of the 3′-end of the T-stretch from the 3′-end of the mature tRNA gene (8–14 bp, as shown). (**A**) Plots showing the fractional distribution of MNase cut sites defining the 3′-boundary of the Tfc1 bootprint for each class. (**B**) Logos showing the location of the T-stretch for each group of genes relative to the first nucleotide of the B-box. The black arrow indicates the location of the major MNase cut site, corresponding to the 3′-boundary of the bootprint (from A); the blue arrow indicates the 3′-end of the mature tRNA, before CCA addition.

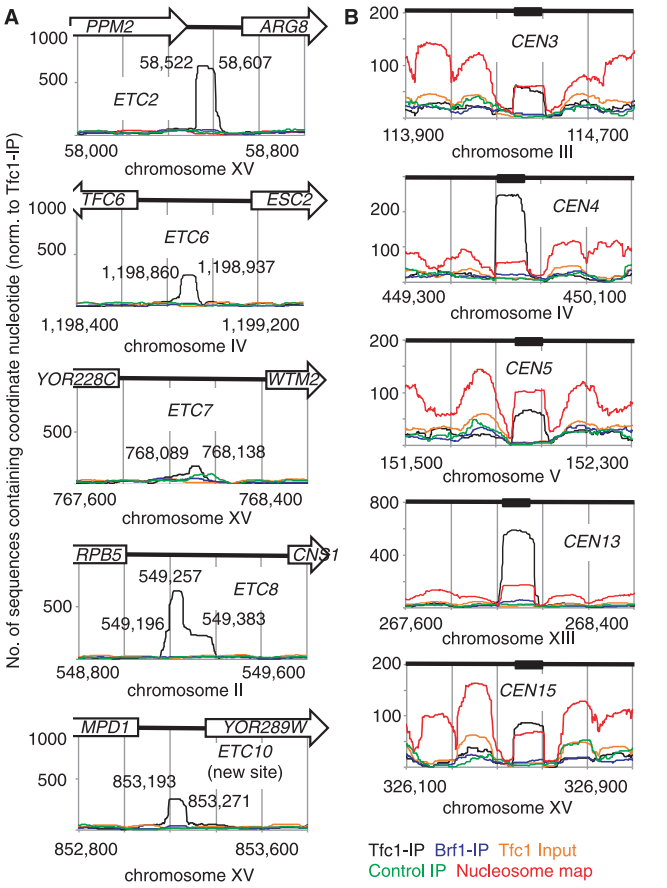


**Figure 5.** TFIIIC binding at *ETC* sites and centromeric nucleosomes. (**A**) Bootprints of five known *ETC* sites and a new *ETC* site. The Tfc1-IP (black), Brf1-IP (blue), control-IP (green) bootprints and Tfc1-input (orange) were normalized to the total number of sequences obtained for the Tfc1-IP. The chromosomal coordinates of the Tfc1 bootprint boundaries are shown. (**B**) Tfc1 physically interacts with five of the 16 *CEN* nucleosomes. The nucleosome map (red line) is superimposed to indicate the correspondence between the square peaks in the nucleosome map and the Tfc1-IP (the actual number of nucleosome sequences containing each base is plotted).

previously (10). Strong signals were observed for the centromeric nucleosomes from chromosomes 4 and 13; weaker signals were observed for those of chromosomes 3, 5 and 15. The IP signals of the *CEN* nucleosomes belonging to the other chromosomes were not significantly above background. Previously, we observed that *CEN* nucleosomes were more sensitive to MNase than canonical nucleosomes (10). Accordingly, the experiment was repeated using significantly less-digested chromatin for the IP. In addition to the *CEN* nucleosomes observed in the first experiment, there were weak signals for the *CEN2* and *CEN11* nucleosomes, but the other *CEN* nucleosomes were not convincingly above background. Significantly, none of the centromeric nucleosomes were detected in the Brf1-IP, except for a weak signal for the *CEN13* nucleosome (Figure 5B). In conclusion, our data provide evidence for a physical interaction between some of the *CEN* nucleosomes and TFIIIC, but not TFIIIB.

## DISCUSSION

We have mapped TFIIIB- and TFIIIC-containing complexes genome-wide *in vivo* with high precision. Our

approach should be of great utility in mapping stable protein–DNA complexes *in vivo*. We have demonstrated that the square peak observed over tRNA genes in our nucleosome map indicates the presence of the TFIIIB–TFIIIC complex, which protects about the same amount of DNA from MNase as a nucleosome. Thus, a protein–DNA complex can masquerade as a nucleosome. However, the TFIIIB–TFIIIC complex was recognizable because of its square peak, which may reflect sequence-specific binding by TFIIIC. Unusual peak shapes in a MNase nucleosome map are therefore useful for detecting specialized chromatin structures, such as the TFIIIB–TFIIIC complex and the centromeric nucleosome.

### Elastic structure of the TFIIIC complex

The TFIIIB–TFIIIC complex is stable *in vitro* (36). Our data indicate that it is also stable *in vivo* because the complexes were isolated after preparing nuclei without formaldehyde cross-linking. In this respect, the TFIIIB–TFIIIC complex resembles the nucleosome, which is also stable. However, in other respects, they are different. The structure of the canonical nucleosome does not suggest any flexibility: a fixed length of DNA is coiled tightly around a central core histone octamer, with strong contacts approximately every 10 bp (1). In contrast, the TFIIIB–TFIIIC complex must exhibit significant flexibility because tRNA genes of different length must be accommodated within the same basic structure, which is anchored on the A and B boxes bound specifically by TFIIIC (2). The terminator might also serve as an anchor point.

Much of the variability in tRNA gene length originates between the A and B boxes, either in the variable arm of the tRNA or due to an intron (Figure 2A). The presence of ~10 extra bp in the variable arm results in a bootprint that is ~10 bp wider, with little cleavage between the A and B boxes, implying that TFIIIC fully protects the additional ~10 bp. The introduction of an extra 10 bp is structurally a challenge and suggests that the TFIIIB–TFIIIC complex has a deformable structure. Intronic DNA, when present, is somewhat protected, but more vulnerable to MNase, suggesting that the TFIIIC structure is elastic enough to accommodate the extra DNA but does not protect it as effectively.

These observations are consistent with biochemical studies of the assembly of TFIIIB–TFIIIC complexes *in vitro* (37) and with electron microscopy studies of TFIIIC bound to a leucyl-tRNA gene with an intron (Supplementary Figure S2), which revealed a dumbbell structure (25). TFIIIC is composed of two lobes, which bind to the A and B boxes; the intervening DNA is relatively extended. The connecting protein between the two lobes is not visible. In some structures though, the lobes appear to coalesce, hiding the intervening DNA, which becomes visible as a loop only if more DNA is artificially inserted between the A and B boxes (25). The latter structure provides the best fit to our data because the intervening DNA is trapped between the two lobes of TFIIIC and so partly protected (Figure 6).

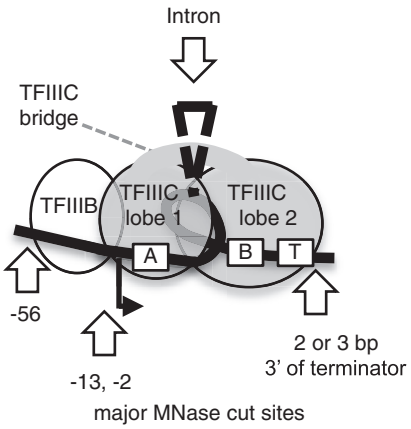


**Figure 6.** Model for the TFIIIB–TFIIIC complex formed on a tRNA gene. Our global bootprint data are consistent with the coalesced 'dumbbell' structure observed for a TFIIIB–TFIIIC–tRNA gene complex in the electron microscope (25). TFIIIC is composed of two lobes connected by a bridge; one lobe binds to the A box, the other to the B box. T: terminator. Arrows: major sites of MNase cleavage.

Thus, our genome-wide data reveal a new dimension to the TFIIIC complex *in vivo*: a naturally elastic structure that can cope with the variability in tRNA gene length. Not only does the TFIIIC complex adapt to variable distances between the A and B boxes, it also accommodates the variable distance of the terminator from the 3′-end of the mature tRNA. The downstream boundary of the complex is fixed ~2 bp downstream of the T-stretch. This interaction might involve the Tfc6 subunit of TFIIIC, which can be cross-linked to the terminator *in vitro* (38,39) and is closely associated with Tfc3, which binds the B box (39), perhaps suggesting additional flexibility in the interaction between these two subunits to accommodate the variation in the distance between the B box and the terminator.

Previous reports showing flexibility in the TFIIIC complex were based on isolated factors and tRNA gene constructs with or without mutations in the intron or upstream *in vitro* (25,37). Those studies revealed flexibility between the B box and the proximal part of the tRNA gene, i.e. in the direction of the A box. The data in the present report are based on global analysis *in vivo* and lead to a model that TFIIIC can accommodate variable lengths of DNA not only between the A and B boxes, but also between the B box and the terminator, perhaps by a looping mechanism (Figure 6). That TFIIIC exhibits flexibility in two directions is a novel finding reported here. Whether this aspect of TFIIIC structure in chromatin is relevant to its other roles at *ETC* sites and centromeres remains to be determined.

### tRNA genes and chromatin organization

tRNA genes can influence local chromatin structure and function. Some tRNA genes repress neighboring genes transcribed by Pol II (5,7) and others act as insulators (3,4), perhaps through their capacity to act as nucleosome phasing barriers (21,22,40). Analysis of our own nucleosome occupancy data confirmed that tRNA genes act

as nucleosome phasing signals in both directions (Supplementary Figure S3). The capacity of tRNA genes to organize nucleosomes probably reflects the stability, high occupancy and fixed position of the TFIIIB–TFIIIC complex.

### TFIIIC physically interacts with some centromeric nucleosomes

A most surprising observation is that centromeric DNA is present in the Tfc1-IP, indicating that Tfc1 interacts with at least five of the 16 centromeres. In all of these cases, the bootprint coincides exactly with the position of the centromeric nucleosome reported previously (10). Thus, it seems likely that the *CEN* nucleosome and the immuno-purified Tfc1 complex observed at the centromere are the same complex. So is Tfc1 a component of the centromeric nucleosome? This seems unlikely because there are no obvious A or B boxes in *CEN* DNA, except for *CEN13*, which has a possible B box (GTTCCGAAC; consensus: GTTCRANYC) overlapping the CBF3 binding site. Instead, we propose that the physical interaction between Tfc1 and centromeric nucleosomes is external to the centromeric nucleosome.

A reasonable hypothesis is that this interaction is mediated through condensin. Condensin is present at TFIIIC binding sites in budding yeast, including tRNA genes (41,42) and it also co-localizes with Ndc10, a subunit of the inner kinetochore, which binds directly to the centromere (43). Some tRNA genes co-localize with the centromere (44,45), in a process mediated by condensin (45). Thus, condensin might form a transient physical link between TFIIIC bound elsewhere and the centromeric nucleosome. Previous TFIIIC ChIP studies (30,31,34) did not detect centromeric DNA, perhaps because multiple formaldehyde cross-links would be required.

Is the TFIIIC at the centromere bound to DNA and, if so, where? The fact that centromeric nucleosomes were not detected in the Brf1-IP implicates sites where only TFIIIC is bound. The *ETC* sites are the most obvious candidates. In budding yeast, nine *ETC* sites have been reported, of which we have confirmed six (although two of these are associated with low levels of TFIIIB) and discovered another (*ETC10*). Thus, our data identify five *ETC* sites lacking TFIIIB. They are located on chromosomes 2 (*ETC8*), 4 (*ETC6*) and 15 (*ETC2*, *ETC7* and *ETC10*). Given that the *CEN* nucleosomes detected in the Tfc1-IP belong to chromosomes 3, 4, 5, 13 and 15, both intra- and interchromosomal interactions are predicted, if the *ETC* sites mediate this interaction. Alternatively, perhaps all TFIIIC binding sites, including tRNA genes, might interact transiently with *CEN* nucleosomes during mitosis. In HeLa cells, TFIIIB and Pol III are displaced during mitosis, but not TFIIIC (46), but it is not known if this is true in yeast.

Interactions between TFIIIC and the centromeric nucleosome may be important in the 3D organization of the nucleus. TFIIIC-mediated interactions with a *CEN* nucleosome within a chromosome would necessarily result in loop formation and a consequent linear condensation. Interchromosomal interactions between TFIIIC and *CEN* nucleosomes could fix chromosomes relative to one another within the nucleus, perhaps contributing to the formation of chromosome territories.

## ACCESSION NUMBERS

GEO database GSE44586.

## SUPPLEMENTARY DATA

Supplementary Data are available at NAR Online.

## ACKNOWLEDGEMENTS

The authors thank the NHLBI DNA Sequencing and Genomics Core Facility (Yoshi Wakabayashi, Yan Luo, Ting Ni and Jun Zhu) for paired-end sequencing and alignments. The authors also thank David Donze and Rohinton Kamakaka for strains.

## FUNDING

Intramural Research program of the NIH (NICHD). Funding for open access charge: National Institutes of Health Intramural Program (NICHD).

*Conflict of interest statement*. None declared.

## REFERENCES

1. Luger,K., Mäder,A.W., Richmond,R.K., Sargent,D.F. and Richmond,T.J. (1997) Crystal structure of the nucleosome core particle at 2.8 Å resolution. *Nature*, **389**, 251–260.
2. Schramm,L. and Hernandez,N. (2002) Recruitment of RNA polymerase III to its target promoters. *Genes Dev.*, **16**, 2593–2620.
3. Donze,D. (2012) Extra-transcriptional functions of RNA polymerase III complexes: TFIIIC as a potential global chromatin bookmark. *Gene*, **493**, 169–175.
4. Kirkland,J.G., Raab,J.R. and Kamakaka,R.T. (2013) TFIIIC bound DNA elements in nuclear organization and insulation. *Biochim. Biophys. Acta*, **1829**, 418–424.
5. Hull,M.W., Erickson,J., Johnston,M. and Engelke,D.R. (1984) tRNA genes as transcriptional repressor elements. *Mol. Cell. Biol.*, **14**, 1266–1277.
6. Kendall,A., Hull,M.W., Bertrand,E., Good,P.D., Singer,R.H. and Engelke,D.R. (2000) A CBF5 mutation that disrupts nucleolar localization of early tRNA biogenesis in yeast also suppresses tRNA gene-mediated transcriptional silencing. *Proc. Natl Acad. Sci. USA*, **97**, 13108–13113.
7. Bolton,E.C. and Boeke,J.D. (2003) Transcriptional interactions between yeast tRNA genes, flanking genes and Ty elements: a genomic point of view. *Genome Res.*, **13**, 254–263.
8. Noma,K., Cam,H.P., Maraia,R.J. and Grewal,S.I. (2006) A role for TFIIIC transcription factor complex in chromosome organization. *Cell*, **125**, 859–872.
9. Cole,H.A., Howard,B.H. and Clark,D.J. (2011) Activation-induced disruption of nucleosome position clusters on the coding regions of Gcn4-dependent genes extends into neighbouring genes. *Nucleic Acids Res.*, **39**, 9521–9535.
10. Cole,H.A., Howard,B.H. and Clark,D.J. (2011) The centromeric nucleosome of budding yeast is perfectly positioned and covers the entire centromere. *Proc. Natl Acad. Sci. USA*, **108**, 12687–12692.
11. Cole,H.A., Nagarajavel,V. and Clark,D.J. (2012) Perfect and imperfect nucleosome positioning in yeast. *Biochim. Biophys. Acta*, **1819**, 639–643.

12. Krassovsky,K., Henikoff,J.G. and Henikoff,S. (2012) Tripartite organization of centromeric chromatin in budding yeast. *Proc. Natl Acad. Sci. USA*, **109**, 243–248.
13. Henikoff,S. and Furuyama,T. (2012) The unconventional structure of centromeric nucleosomes. *Chromosoma*, **121**, 341–352.
14. Rusché,L.N., Kirchmaier,A.L. and Rine,J. (2002) Ordered nucleation and spreading of silenced chromatin in *Saccharomyces cerevisiae*. *Mol. Biol. Cell.*, **13**, 2207–2222.
15. Kleinschmidt,R.A., LeBlanc,K.E. and Donze,D. (2011) Autoregulation of an RNA polymerase II promoter by the RNA polymerase III transcription factor III C (TF(III)C) complex. *Proc. Natl Acad. Sci. USA*, **108**, 8385–8389.
16. Li,H. and Durbin,R. (2009) Fast and accurate short read alignment with Burrows-Wheeler Transform. *Bioinformatics*, **25**, 1754–1760.
17. Langmead,B. and Salzberg,S.L. (2012) Fast gapped-read alignment with Bowtie 2. *Nat. Methods*, **9**, 357–359.
18. Lowe,T.M. and Eddy,S.R. (1997) tRNAscan-SE: a program for improved detection of transfer RNA genes in genomic sequence. *Nucleic Acids Res.*, **25**, 955–964.
19. Crooks,G.E., Hon,G., Chandonia,J.M. and Brenner,S.E. (2004) WebLogo: A sequence logo generator. *Genome Res.*, **14**, 1188–1190.
20. Parnell,T.J., Huff,J.T. and Cairns,B.R. (2008) RSC regulates nucleosome positioning at Pol II genes and density at Pol III genes. *EMBO J.*, **27**, 100–110.
21. Mavrich,T.N., Ioshikhes,I.P., Venters,B.J., Jiang,C., Tomsho,L.P., Qi,J., Schuster,S.C., Albert,I. and Pugh,B.F. (2008) A barrier nucleosome model for statistical positioning of nucleosomes throughout the yeast genome. *Genome Res.*, **18**, 1073–1083.
22. Jiang,C. and Pugh,B.F. (2009) A compiled and systematic reference map of nucleosome positions across the *Saccharaomyces cerevisiae* genome. *Genome Biol.*, **10**, R109.
23. Engelke,D.R., Ng,S., Shastry,B.S. and Roeder,R.G. (1980) Specific interaction of a purified transcription factor with an internal control region of 5S RNA genes. *Cell*, **19**, 717–728.
24. Kassavetis,G.A., Bartholomew,B., Blanco,J.A., Johnson,T.E. and Geiduschek,E.P. (1991) Two essential components of the *Saccharomyces cerevisiae* transcription factor TFIIIB: transcription and DNA-binding properties. *Proc. Natl Acad. Sci. USA*, **88**, 7308–7312.
25. Schultz,P., Marzouki,N., Marck,C., Ruet,A., Oudet,P. and Sentenac,A. (1989) The two DNA-binding domains of yeast transcription factor tau as observed by scanning transmission electron microscopy. *EMBO J.*, **8**, 3815–3824.
26. Kassavetis,G.A., Braun,B.R., Nguyen,L.H. and Geiduschek,E.P. (1990) *S. cerevisiae* TFIIIB is the transcription initiation factor proper of RNA polymerase III, while TFIIIA and TFIIIC are assembly factors. *Cell*, **60**, 235–245.
27. Allison,D.S. and Hall,B.D. (1985) Effects of alterations in the 3′ flanking sequence on *in vivo* and *in vitro* expression of the yeast *SUP4*-o tRNATyr gene. *EMBO J.*, **4**, 2657–2664.
28. Hamada,M., Sakulich,A.L., Koduru,S.B. and Maraia,R.J. (2000) Transcription termination by RNA polymerase III in fission yeast. A genetic and biochemically tractable model system. *J. Biol. Chem.*, **275**, 29076–29081.
29. Braglia,P., Percudani,R. and Dieci,G. (2005) Sequence context effects on oligo(dT) termination signal recognition by *Saccharomyces cerevisiae* RNA polymerase III. *J. Biol. Chem.*, **280**, 19551–19562.
30. Roberts,D.N., Stewart,A.J., Huff,J.T. and Cairns,B.R. (2003) The RNA polymerase III transcriptome revealed by genome-wide localization and activity-occupancy relationships. *Proc. Natl Acad. Sci. USA*, **100**, 14695–14700.
31. Moqtaderi,Z. and Struhl,K. (2004) Genome-wide occupancy profile of the RNA polymerase III machinery in *Saccharomyces cerevisiae* reveals loci with incomplete transcription complexes. *Mol. Cell. Biol.*, **24**, 4118–4127.
32. Guffanti,E., Percudani,R., Harismendy,O., Soutorina,J., Wener,M., Iacovella,M.G., Negri,R. and Dieci,G. (2006) Nucleosome depletion activates poised RNA polymerase III at unconventional transcription sites in *Saccharomyces cerevisiae*. *J. Biol. Chem.*, **281**, 23945–23957.
33. Valenzuela,L., Dhillon,N. and Kamakaka,R.T. (2009) Transcription independent insulation at TFIIIC-dependent insulators. *Genetics*, **183**, 131–148.
34. Harismendy,O., Gendrel,C.G., Soularue,P., Gidrol,X., Sentenac,A., Werner,M. and Lefebvre,O. (2003) Genome-wide location of yeast RNA polymerase III transcription machinery. *EMBO J.*, **22**, 4738–4747.
35. Venters,B.J., Wachi,S., Mavrich,T.N., Andersen,B.E., Jena,P., Sinnamon,A.J., Jain,P., Rolleri,N.S., Jiang,C., Hemeryck-Walsh,C. *et al.* (2011) A comprehensive genomic binding map of gene and chromatin regulatory protein in *Saccharomyces*. *Mol. Cell*, **41**, 480–492.
36. Lefebrve,O., Rüth,J. and Sentenac,A. (1994) A mutation in the largest subunit of yeast TFIIIC affects tRNA and 5S RNA synthesis. *J. Biol. Chem.*, **269**, 23374–23381.
37. Joazeiro,C.A.P., Kassavetis,G.A. and Geiduschek,E.P. (1996) Alternative outcomes in assembly of promoter complexes: the roles of TBP and a flexible linker in placing TFIIIB on tRNA genes. *Genes Dev.*, **10**, 725–739.
38. Braun,B.R., Bartholomew,B., Kassavetis,G.A. and Geiduschek,E.P. (1992) Topography of transcription factor complexes on the *Saccharomyces cerevisiae* 5S RNA gene. *J. Mol. Biol.*, **228**, 1063–1077.
39. Huang,Y. and Maraia,R.J. (2001) Comparison of the RNA polymerase III transcription machinery in *Schizosaccharomyces pombe*, *Saccharomyces cerevisiae* and human. *Nucleic Acids Res.*, **29**, 2675–2690.
40. Morse,R.H., Roth,S.Y. and Simpson,R.T. (1992) A transcriptionally active tRNA gene interferes with nucleosome positioning *in vivo*. *Mol. Cell. Biol.*, **12**, 4015–4025.
41. D'Ambrosio,C., Schmidt,C.K., Katou,Y., Kelly,G., Itoh,T., Shirahige,K. and Uhlmann,F. (2008) Identification of *cis*-acting sites for condensin loading onto budding yeast chromosomes. *Genes Dev.*, **22**, 2215–2227.
42. Haeusler,R.A., Pratt-Hyatt,M., Good,P.D., Gipson,T.A. and Engelke,D.R. (2008) Clustering of yeast tRNA genes is mediated by specific association of condensin with tRNA gene transcription complexes. *Genes Dev.*, **22**, 2204–2214.
43. Bachellier-Bassi,S., Gadal,O., Bourout,G. and Nehrbass,U. (2008) Cell cycle-dependent kinetochore localization of condensin complex in *Saccharomyces cerevisiae*. *J. Struc. Biol.*, **162**, 248–259.
44. Duan,Z., Andronescu,M., Schutz,K., McIlwain,S., Kim,Y.J., Lee,C., Shendure,J., Fileds,S., Blau,C.A. and Noble,W.S. (2010) A three-dimensional model of the yeast genome. *Nature*, **465**, 363–367.
45. Iwasaki,O., Tanaka,A., Tanizawa,H., Grewal,S.I.S. and Noma,K. (2010) Centromeric localization of dispersed Pol III genes in fission yeast. *Mol. Biol. Cell.*, **21**, 254–265.
46. Fairley,J.A., Scott,P.H. and White,R.J. (2003) TFIIIB is phosphorylated, disrupted and selectively released from tRNA promoters during mitosis *in vivo*. *EMBO J.*, **22**, 5841–5850.